Adaptive piezoelectric shunt damping

A J Fleming[1] and S O R Moheimani

School of Electrical Engineering and Computer Science, University of Newcastle,
Callaghan 2308, Australia

E-mail: andrew@ee.newcastle.edu.au

Abstract
Piezoelectric shunt damping systems reduce structural vibration by shunting
an attached piezoelectric transducer with an electrical impedance. Current
impedance designs result in a coupled electrical resonance at the target
modal frequencies. In practical situations, variation in structural load or
environmental conditions can result in significant changes in the structural
resonance frequencies. This variation can severely reduce shunt damping
performance as the electrical impedance remains tuned to the nominal
resonance frequencies. This paper introduces a method for online adaptation
of the shunting impedance. A reconstructed estimate of the RMS strain is
minimized by varying the component values of a synthetic shunt damping
circuit. The techniques presented are applied in real time to tune the
component values of a randomly excited beam.

(Some figures in this article are in colour only in the electronic version)

1. Introduction

Today's increasingly high speed and lightweight structures are
subject to extensive vibrations that can reduce structural life
and contribute to mechanical failure. Piezoelectric transducers
(PZTs), in conjunction with appropriate circuitry, can be used
as a mechanical energy dissipation device. If a simple resistor
is placed across the terminals of the PZT, the PZT will act as
a viscoelastic damper [2]. If the network consists of a series
inductor–resistor R–L circuit, the passive network combined
with the inherent capacitance of the PZT creates a damped
electrical resonance. The resonance can be tuned so that the
PZT acts as a tuned vibrational energy absorber [2]. Wu [3]
reports a method for damping multiple vibration modes with a
single PZT. The circuit requires as many R–L parallel branches
as there are modes to be controlled. Each branch also contains
'current blocking' networks, each consisting of an inductor and
capacitor connected in parallel to isolate adjacent branches.
Passive shunt damping is regarded as a simple, low cost, light
weight, and easy to implement method of controlling structural
vibrations.

In practical situations, variation in structural load or
environmental conditions can result in significant movement
of the structural resonance frequencies. Such variation
can severely reduce shunt damping performance as the

electrical impedance remains tuned to the nominal resonance
frequencies. This problem was first addressed in [4], where
a viscoelastic spring, with temperature-dependent stiffness,
was used as a tuned mechanical absorber. Hollkamp [5]
later proposed a similar methodology for piezoelectric shunt
damping. A mechanically driven resistor was used to vary
the virtual inductance of a single mode shunt damping circuit.
The performance function, related to the RMS strain, was
estimated using an additional piezoelectric patch. In this paper
we consider the effect of broadband disturbances on structures
with multiple high profile modes. Another approach, based
on capacitive shunting, considers tonal disturbances and
structures with a single dominant lightly damped mode [6].
In situations involving non-sinusoidal disturbances, such
techniques are deemed undesirable as the structural response
is increased outside of the damped region.

Recently, a new method for implementing shunt damping
circuits has been introduced. The *synthetic impedance* [7–
9] uses a voltage controlled current source and DSP system
to implement the terminal impedance of an arbitrary shunt
network. It replaces physical circuits to provide effective
structural damping whilst avoiding the problems encountered
with direct circuit implementation. Because the desired
impedance is now defined only by the DSP system transfer
function, the component values are easily modified online.

This paper introduces a technique for online adaptation
of shunt network component values. A single piezoelectric

---

[1] Author to whom any correspondence should be addressed.

patch is used to simultaneously damp multiple modes of a mechanical system and to procure a performance function estimate. Experimental results are presented for a randomly excited, simply supported beam. The second and third modes of the beam are controlled with an attached PZT and adaptive shunt damping system. The algorithm is shown to regain optimal damping performance after severely detuning the component values.

The paper is presented in six sections. We begin with a brief review of piezoelectric shunt circuit design and a description of the synthetic impedance. In section 3 we will discuss the modelling of structural dynamics and show how to model the presence of an electrical shunt impedance. The adaptive impedance is introduced in section 4. Experimental and theoretical results are presented in section 5. We conclude with a review of the initial goals, a summary of the results, and some future directions for research on adaptive shunt damping.

2. Piezoelectric shunt damping

Shunt damping methodologies are often grouped into two broad categories: single mode and multi-mode. Single-mode shunt damping techniques are simple but damp only one structural mode for every PZT. Multiple-mode shunt damping techniques require more complicated shunt circuits but are capable of damping many modes.

2.1. Single-mode shunt damping

Single-mode damping was introduced to decrease the magnitude of one structural mode [10]. Two examples of single-mode damping are shown in figure 1: parallel and series shunt damping. The combination of an R–L shunt circuit combined with the intrinsic capacitance of the PZT introduces an electrical resonance. This can be tuned to one structural mode in a manner analogous to that of a mechanical vibration absorber. Single-mode damping can be applied to reduce several structural modes with the use of as many piezoelectric patches and damping circuits as necessary.

Problems may result if these piezoelectric patches are bonded to, or imbedded in the structure. First, the structure may not have sufficient room to accommodate all of the patches. Second, the structure may be altered or weakened when the piezoelectric patches are applied. In addition, a large number of patches can increase the structural weight, making it unsuitable for applications such as aerospace.

2.2. Multiple-mode shunt damping

To alleviate the problems associated with single-mode damping, multi-mode shunt damping has been introduced; i.e. the use of one piezoelectric patch to damp several structural modes. Two multi-mode shunt damping methodologies will be discussed: current blocking techniques, as presented in [3, 11–13], and current flowing techniques, as presented in [1, 14].

2.2.1. Current blocking techniques.
The principle of multi-mode shunt damping is to insert a *current blocking* network [3, 11–13] in series with each shunt branch. In figure 2, the blocking circuit consists of a capacitor and
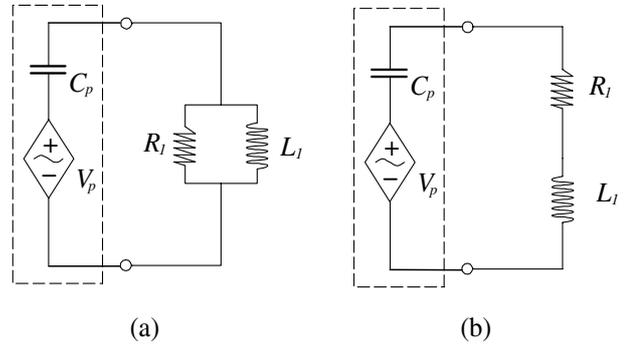

Figure 1. Series (a), and parallel (b), single-mode shunt damping circuits shown connected to a PZT transducer.

inductor in parallel, C_3–L_3. The number of antiresonant circuits in each R–L shunt branch increases with the number of structural modes to be damped simultaneously. Each R–L shunt branch is designed to damp one structural mode. For example, R_1–L_1 in figure 2 is tuned to resonate at ω_1, the resonance frequency of the first structural mode to be damped. R_2–L_2 is tuned to ω_2, the second structural mode to be damped, and so on.

According to Wu [3], the inductance values for the shunt circuits shown in figure 2 can be calculated from the following expressions (it is assumed that $\omega_1 < \omega_2$):

$$L_1 = \frac{1}{\omega_1^2 C_p} \qquad \tilde{L}_2 = \frac{1}{\omega_2^2 C_p} \qquad L_3 = \frac{1}{\omega_1^2 C_3}$$

$$L_2 = \frac{(L_1\tilde{L}_2 + \tilde{L}_2 L_3 - L_1 L_3 - \omega_2^2 L_1 \tilde{L}_2 L_3 C_3)}{(L_1 - \tilde{L}_2)(1 - \omega_2^2 L_3 C_3)} \tag{1}$$

where C_p is the capacitance of the PZT, and C_3 is an arbitrary capacitor used in the current blocking network.

2.2.2. Current flowing techniques.
More recently, the *current flowing* shunt circuit has been introduced [1, 14]. Shown in figure 3, the current flowing circuit requires one circuit branch for each structural mode to be controlled. The current flowing $\hat{L}_i$–C_i network in each branch is tuned to approximate a short circuit at the target resonance frequency whilst approximating an open circuit at the adjacent branch frequencies. The remaining inductor and resistor in each branch $\tilde{L}_i$–R_i, is tuned to damp the ith target structural mode in a manner analogous that performed during single-mode design, i.e. the current flowing network decouples the multi-mode problem into a number of effectively independent single-mode designs. Unlike current blocking techniques, the order of each current flowing branch does not increase as the number of modes to be shunt damped simultaneously increases. Besides greatly simplifying the tuning procedure, the current flowing technique requires less components and gracefully extends to damp a large number of modes simultaneously, e.g. five modes of a simply supported plate [14]. Further practical advantages are realized when implementing the circuit; only a single non-floating inductor is required per branch [14]. A similar technique can be found in [15].
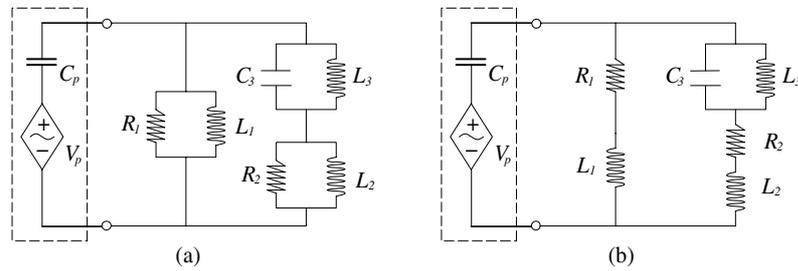
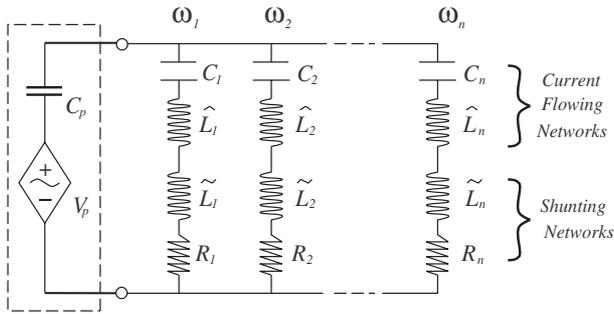**Figure 2.** Parallel (a), and series (b), multi-mode shunt damping circuits shown connected to a PZT transducer.

Figure 3. Current flowing piezoelectric shunt damping circuit [1] shown connected to a PZT transducer.

Figure 4. Functionality of the synthetic impedance.

2.3. Implementation difficulties

Currently shunt damping circuits are implemented using a network of physical components. There are a number of problems associated with *direct circuit* implementation, the foremost of which are listed below.

- Typically the shunt circuits require large inductor values (up to thousands of henries). Virtual grounded and floating inductors (Riordan gyrators [16]) are required to implement the inductor elements. Such virtual implementations are typically poor representations of ideal inductors. They are large in size, difficult to tune, and are sensitive to component age, temperature, and non-ideal characteristics.

- Piezoelectric patches are capable of generating hundreds of volts for moderate structural excitations. This requires the entire circuit to be constructed from high voltage components. Further voltage limitations arise due to the internal gains of the virtual inductors.

- The minimum number of opamps required to implement the shunt damping circuit increases rapidly with the number of modes to be damped. At least 30 opamps are required to implement a series configuration multi-mode shunt damping circuit with current blocking networks in every branch. The relationship between the number of opamps and the number of modes to be damped for this circuit configuration is given by $No\ opamps = 2n + 4n(n-1)$, where n is the number of modes to be damped. Current flowing techniques require a considerably smaller number of opamps, $No\ opamps = 2n$, but still suffer from the previous two difficulties.
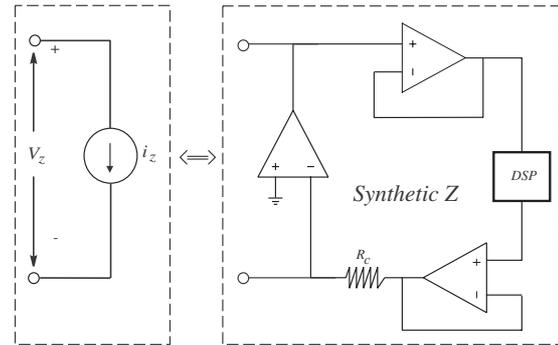
2.4. The synthetic impedance

It should be clear that, although the concept of multi-mode shunt damping is useful, in practice, implementation difficulties make its application somewhat limited. The synthetic impedance [7–9] allows the implementation of complicated multi-mode shunt damping circuits using only a few opamps, one resistor, and a digital signal processor (DSP).
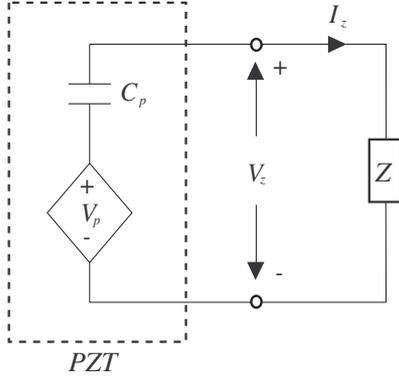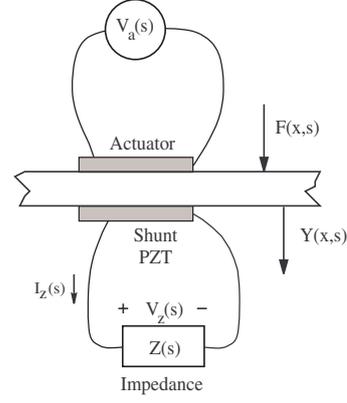
The synthetic impedance is a two-terminal device that establishes an arbitrary relationship between voltage and current at its terminals [8]. The functionality is shown in figure 4, where $i_z(t) = f(v_z(t))$. This can be made to synthesize any network of physical components by fixing i_z to be the output of a linear transfer function with input v_z, i.e.

$$I_z(s) = Y(s)V_z(s) \qquad (2)$$

where $Y(s) \equiv \frac{1}{Z(s)}$ and $Z(s)$ is the impedance to be seen from the terminals.

3. Modelling the compound system

For generality, we will enter the modelling process with knowledge *a priori* of the system dynamics. As an example, we consider a simply supported beam with two bonded piezoelectric patches, one to be used as a source of disturbance, and the other for shunt damping. The transfer function $G_{vv}(s)$ from an applied actuator to sensor voltage can be derived analytically from the Euler–Bernoulli beam equation [17], or obtained experimentally through system identification [18]. Using similar methods, we may obtain the transfer function from an applied actuator voltage to the displacement at a point $G_{yv}(x, s)$.

Figure 5. Series electrical model of a PZT.

Following the modal analysis procedure [19], the resulting transfer functions have the familiar form:

$$G_{yv}(x, s) \triangleq \frac{Y(x, s)}{V_a(s)} = \sum_{i=1}^{\infty} \frac{F_i \phi_i(x)}{s^2 + 2\zeta_i w_i s + w_i^2} \qquad (3)$$

$$G_{vv}(s) \triangleq \frac{V_s(s)}{V_a(s)} = \sum_{i=1}^{\infty} \frac{\alpha_i}{s^2 + 2\zeta_i w_i s + w_i^2} \qquad (4)$$

where $Y(x, s)$ is the measured displacement, $V_s(s)$ is the piezoelectric sensor voltage, and $V_a(s)$ is the voltage applied to a collocated actuator. F_i, and α_i represent the lumped modal and piezoelectric constants applicable to the ith mode of vibration.

3.1. Piezoelectric modelling

Piezoelectric crystals have a three-dimensional structure, i.e. crystal deformation occurs in three dimensions. Practical mechanical applications require the effect in one or two dimensions only. This can be achieved by manufacturing piezoelectric patches with large length and width to thickness ratios.

PZTs behave electrically like a capacitor and mechanically like a stiff spring [20]. An equivalent electrical model has been presented [2, 21–23], and is widely used in the literature. The model, shown in figure 5, consists of a strain-dependent voltage source and series capacitor.

3.2. Modelling the presence of a shunt circuit

Consider figures 5 and 6 where a piezoelectric patch is shunted by an impedance Z. The current–voltage relationship can be represented in the Laplace domain as

$$V_z(s) = I_z(s) Z(s) \qquad (5)$$

where $V_z(s)$ is the voltage across the impedance and $I_z(s)$ is the current flowing through the impedance. Using Kirchhoff's voltage law on the circuit shown in figure 5 we obtain

$$V_z(s) = V_p(s) - \frac{1}{C_p s} I_z(s) \qquad (6)$$

where V_p is the voltage induced by the electromechanical coupling effect [2] and C_p represents the capacitance of the

Figure 6. Structural input/outputs.

shunting layer. Combining (5) and (6) we obtain

$$V_z(s) = \frac{Z(s)}{\frac{1}{C_p s} + Z(s)} V_p(s) \qquad (7)$$

or

$$V_z(s) = \frac{C_p s Z(s)}{1 + C_p s Z(s)} V_p(s). \qquad (8)$$

Notice that when $Z = \infty$, i.e. open-circuit, we have

$$Z = \infty \Rightarrow V_z(s) \triangleq V_p(s) = G_{vv}(s) V_a(s). \qquad (9)$$

However, if the circuit is shunted by a finite impedance Z, by linearity, we may write

$$V_p(s) = G_{vv}(s) V_a(s) - G_{vv}(s) V_z(s) \qquad \text{s.t. } Z \neq \infty, 0. \qquad (10)$$

The above equations (9) and (10) are reported in state-space form [24] as the *sensing* and *actuator equations*. By substituting (7) into (10),

$$V_p(s) = G_{vv}(s) V_a(s) - G_{vv}(s) \frac{Z(s)}{\frac{1}{C_p s} + Z(s)} V_p(s). \qquad (11)$$

Then by rearranging we find the shunt damped transfer function

$$\frac{V_p(s)}{V_a(s)} = \frac{G_{vv}(s)}{1 + G_{vv}(s) K(s)} \qquad (12)$$

where

$$K(s) = \frac{Z(s)}{Z(s) + \frac{1}{C_p s}}. \qquad (13)$$

Note that $V_p(s)$ is dynamically equivalent to $V_s(s)$ (i.e. the open-circuit voltage). We can rewrite the shunt damped or closed loop transfer functions as

$$\tilde{G}_{vv}(s) \triangleq \frac{V_s(s)}{V_a(s)} = \frac{G_{vv}(s)}{1 + G_{vv}(s) K(s)} \qquad (14)$$

and

$$\tilde{G}_{yv}(x, s) \triangleq \frac{Y(x, s)}{V_a(s)} = \frac{G_{yv}(x, s)}{1 + G_{vv}(s) K(s)}. \qquad (15)$$

From equations (14) and (15) we observe that shunt damping is equivalent to a negative feedback control strategy parameterized in Z.

Using a similar procedure and the principle of superposition, the effect of a generally distributed disturbance force can be included:

$$V_s(s) = \frac{G_{vf}(s)F(x,s)}{1 + K(s)G_{vv}(s)} + \frac{G_{vv}(s)V_{in}(s)}{1 + K(s)G_{vv}(s)} \quad (16)$$

$$Y(x,s) = \frac{G_{yf}(x,s)F(x,s)}{1 + K(s)G_{vv}(s)} + \frac{G_{yv}(x,s)V_{in}(s)}{1 + K(s)G_{vv}(s)}. \quad (17)$$

4. Adaptive shunt damping

Before service, shunt circuits are tuned to the structural resonance frequencies of interest. To maintain some kind of optimal performance, we introduce a technique for online tuning of the component values. This technique utilizes the synthetic impedance along with time varying transfer functions to alter the parameters of a shunt circuit in real time.

4.1. System schematic

We will first derive the damped system transfer function from an applied actuator voltage to the measured output V_z. From section 3.2 we have

$$V_p(s) = G_{vv}(s)V_a(s) - G_{vv}(s)V_z(s) \qquad \text{s.t. } Z \neq \infty, 0. \quad (18)$$

$$V_z(s) = \frac{C_p s Z(s)}{1 + C_p s Z(s)} V_p(s). \quad (19)$$

By rearranging (19),

$$V_p(s) = \frac{1 + C_p s Z(s)}{C_p s Z(s)} V_z(s) \quad (20)$$

and substituting into (18), the internal variable $V_p(s)$ can be eliminated to find the damped system transfer function

$$\frac{V_z(s)}{V_a(s)} = \frac{K(s)G_{vv}(s)}{1 + K(s)G_{vv}(s)} \quad (21)$$

where

$$K(s) = \frac{C_p s Z(s)}{1 + C_p s Z(s)}. \quad (22)$$

Using a similar procedure and the principle of superposition the effect of a generally distributed disturbance force $F(x,s)$ can be included:

$$V_z(s) = \frac{K(s)G_{vf}(s)F(x,s)}{1 + K(s)G_{vv}(s)} + \frac{K(s)G_{vv}(s)V_a(s)}{1 + K(s)G_{vv}(s)}. \quad (23)$$

Note that the output $V_z(s)$ offers little information about the performance of the controller. Traditionally, designers seek to minimize the output magnitude resulting from some disturbance profile. In this case the controller is performing well when there is a lightly damped electrical resonance between the impedance and the PZT at the resonance frequencies. Hence a large measured output can signify a large reduction in structural vibration.

A useful performance signal is the displacement at a point or the equivalent sensor voltage V_p. Both of these quantities are dynamically related to the measured output V_z but are parameterized in terms of the impedance $Z(s)$, for
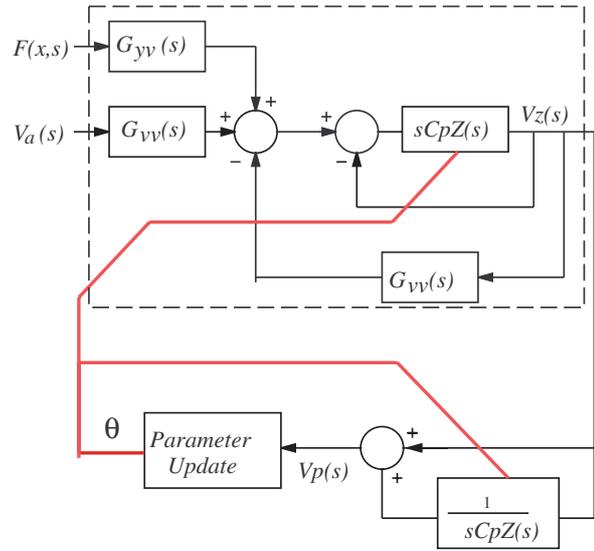
Figure 7. Schematic block diagram of the adaptive shunt damped system.

example (20). This means that, to implement an adaptive piezoelectric shunt damping system, we need to synthesize the impedance $Z(s)$ twice: firstly to implement the shunt damping circuit, and secondly to reconstruct the performance signal V_p. A schematic block diagram is shown in figure 7 where the broken line represents the damped system boundary.

4.2. Comparison to existing adaptive frameworks

Consider the adaptive feedback configuration shown in figure 7. This bears little resemblance to conventional LMS based feedback control systems [25] for the following reasons:

- The feedback path is not affine in the manipulated transfer function $Z(s, \theta)$.
- The transfer function $Z(s, \theta)$ is rigidly parameterized and spans only a small subset of $\mathcal{G}_s^n$, the set of all stable transfer functions of degree n. This is because $Z(s, \theta)$ implements a passive circuit of fixed structure. Although this restriction complicates the performance surface[2], it also guarantees closed loop stability [26] and involves fewer optimization arguments.
- The secondary path is parameterized in terms of θ and the manipulated transfer function $Z(s, \theta)$.

In summary, by using a controller of fixed structure, we have retained the known benefits of shunt damping, but have complicated the analysis. A simple parameterization and update algorithm will now be presented.

4.3. Impedance parameterization

Consider the current blocking multi-mode shunt circuit shown in figure 2. This circuit can be parameterized in terms of the branch resistances and resonance frequencies. Unfortunately each branch is not only parameterized in terms of its own

---

[2] As opposed to the performance surfaces discussed in [25] that have certain geometric properties, such as convexity. These properties can be exploited to facilitate simplified convergence analysis and parameter optimization.
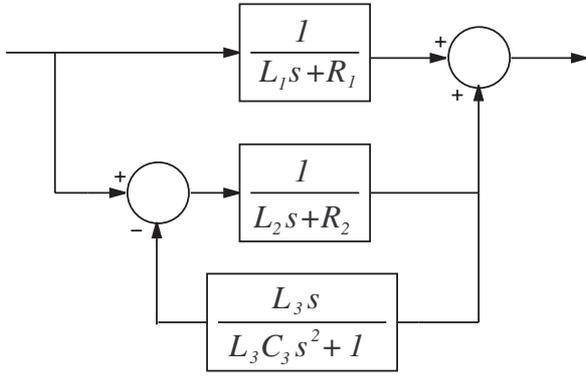
Figure 8. Admittance block diagram of a series two-mode shunt damping circuit.

resonance frequency but also the resonance frequencies of other branches (due to the current blockers). The result is an overly complicated expression for each inductor in terms of the desired branch frequencies and can be simplified by explicitly parameterizing the current blocking network and using the results of [8] to generate an equivalent block diagram that can be implemented in real time. Figure 8 shows[3] $Y(s)$, the admittance of a series configuration two-mode shunt damping circuit, explicitly broken up into each R–L branch resonance pair and L–C current blocker. The relationship between the parameter vector θ and the component values is shown in equation (1):

$$\theta = [\omega_1 \, \omega_2 \cdots \omega_{N_\omega}]. \tag{24}$$

Alternatively, if a current flowing configuration is to be employed, the components and admittance of each branch can be easily parameterized in terms of the circuit's target resonance frequencies [1, 14]. In this case the total admittance of the circuit is simply the sum of a number of second-order admittances.

4.4. Performance evaluation

Conventional adaptive feedback control architectures generally make use of a synthesized reference signal to estimate the performance of the controller [25]. In this case, an estimate of the nominal sensitivity function $\frac{Y(j\omega)}{D_o(j\omega)}$ is available, where $Y(s)$ is the system output and $D_o(s)$ is the synthesized disturbance. Currently, for the architecture shown in figure 7, there is no such method for obtaining an estimate of the disturbance. The difficulty is due to the parameterization of the secondary path in the unknown plant we are trying to control. It may be possible to estimate the unknown dynamics of the secondary path on-line (as in [27]), but this is considered an impractical approach to the problem.

Another technique for evaluating the performance of the controller is to estimate certain statistical properties of the disturbance, and use only the system output as a reference. For example, consider some transfer function $G(s)$ with output $Y(s)$, excited by $u(t)$, a stationary random process with constant power spectral density α. The RMS value of the

---

[3] $Y(s)$ is the admittance used to implement $Z(s)$ in the synthetic impedance. Refer to section 2.4.

output and the $\mathcal{H}_2$ norm of the system can be computed using the following relations:

$$S_Y(\omega) = |G(j\omega)|^2 S_U(\omega) \tag{25}$$

$$E\{y(t)^2\} = \int_{-\infty}^{\infty} y^2(t)\, \mathrm{d}t \tag{26}$$

$$= \frac{1}{2\pi} \int_{-\infty}^{\infty} S_Y(\omega)\, \mathrm{d}\omega \tag{27}$$

$$\|G(j\omega)\|_2^2 = \frac{1}{2\pi} \int_{-\infty}^{\infty} |G(j\omega)|^2\, \mathrm{d}\omega \tag{28}$$

$$= \frac{1}{2\pi} \int_{-\infty}^{\infty} \frac{S_Y(\omega)}{S_U(\omega)}\, \mathrm{d}\omega. \tag{29}$$

For our example system, the quantity $\int_{-\infty}^{\infty} S_Y(\omega)\, \mathrm{d}\omega$ is directly proportional to $\|G(j\omega)\|_2^2$ and $E\{y(t)^2\}$.

4.4.1. The performance function. Two performance functions will be presented: the RMS strain $V^{strain}(\theta)$, and the ratio of RMS strain to RMS shunt voltage $V^{ratio}(\theta)$. The former is the obvious choice but is prone to errors due to a dependence on the power of the disturbance. The latter is an approximate method for minimizing the RMS strain, but achieves a degree of isolation from the stochastic characteristics of the disturbance.

RMS strain. The objective will be to minimize $E\{V_p(t)^2\}$, i.e. to minimize the RMS strain at the PZT ($V_p(t)$ is dynamically proportional to the strain under the piezoelectric patch). The signal $V_p(t)$ can be synthesized in real time from the shunt voltage (20) as discussed in section 4.1:

$$\theta^* = \arg\min_{\theta \in \mathfrak{R}^{N_\omega}} V^{strain}(\theta) \tag{30}$$

$$= \arg\min_{\theta \in \mathfrak{R}^{N_\omega}} E\{V_p^2(t)\}. \tag{31}$$

The performance function $V^{strain}(\theta)$ is approximated by its discrete time equivalent:

$$V_k^{strain}(\theta) = \frac{1}{N} \sum_{i=kN}^{(k+1)N-1} V_p^2(iT_s) \tag{32}$$

where T_s is the sampling interval and N is the number of samples in each kth record interval. The corresponding closed loop system norm interpretation is

$$\theta^* = \arg\min_{\theta \in \mathfrak{R}^{N_\omega}} \|G(j\omega, \theta)\|_{2.W(\omega)}^2 \tag{33}$$

$$= \arg\min_{\theta \in \mathfrak{R}^{N_\omega}} \frac{1}{2\pi} \int_{-\infty}^{\infty} W(\omega)|G(j\omega, \theta)|^2\, \mathrm{d}\omega \tag{34}$$

where in this case, $G(j\omega, \theta)$ is the closed loop transfer function from disturbance to V_p, and $W(\omega)$ is a weighting function equal to $S_U(\omega)$.

The disturbance signal must be stationary so that the performance estimates $V_k(\theta), V_{k+1}(\theta), \ldots, V_{k+M}(\theta)$ are consistent and unbiased. We refer to the term 'stationary' as 'wide-sense stationary' [28] relative to N, e.g. stationary over the interval $T_s[kN(k+M)N-1]$.

If V_p is stationary, $V_k(\theta)$ can be shown to be a consistent and unbiased estimator over a single record interval. The requirement for stationarity is extended to M such intervals so that there will be at least M consecutive estimates of $V(\theta)$ with similar disturbance. In practice, the encountered size of M will define the amount of noise and bias in the gradient estimates.
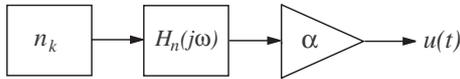
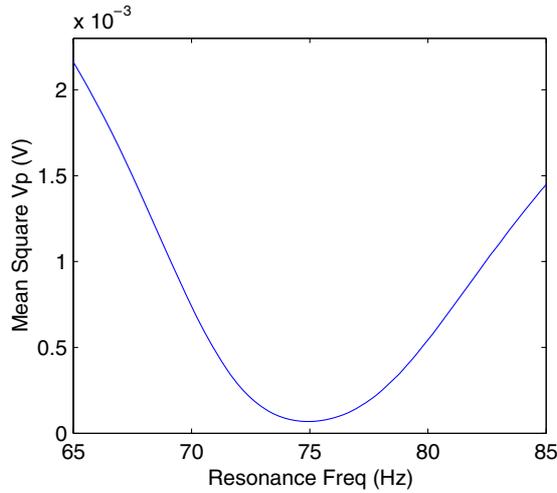**Figure 9.** Disturbance noise model.

Figure 10. The performance function plotted against the second mode resonance frequency. The excitation is a zero mean stationary random process.

RMS ratio. If the disturbance is not sufficiently stationary, the above performance function will not provide a useful estimate of the damping performance. Consider the model of a disturbance shown in figure 9, where n_k is a white noise source, $H_n(j\omega)$ is a noise filter, and α is a slowly time varying gain. Although the signal $u(t)$ is not stationary, if the gain α varies sufficiently slowly, the power spectral density of adjacent record intervals will differ only by a constant gain α^2. The aim is to define a performance function independent of α^2.

Consider the performance function (35):

$$V_k^{ratio}(\theta) = \frac{\sum_{i=kN}^{(k+1)N-1} V_p^2(iT_s)}{\sum_{i=kN}^{(k+1)N-1} V_R^2(iT_s)} \qquad (35)$$

where V_R is the voltage across the shunting resistor. As both of the impedance structures, current blocking and current flowing, approximate a series inductor and resistor around a specific resonance frequency, we can estimate the signal V_R for each of the shunt branches by filtering the shunt voltage

$$V_R(s) = V_z(s)\frac{R}{Ls + R} \qquad (36)$$

where L is the inductor value currently being implemented. For multiple modes the performance function can be decomposed into its modal components by appropriately pre-filtering V_z. Intuitively, by minimizing $V_k^{ratio}(\theta)$ we are minimizing the RMS strain and maximizing the voltage across the shunting resistance. Maximizing the voltage across a shunt resistance will maximize the amount of dissipated energy. For any given disturbance, both the numerator and denominator are linear in α^2 and hence the performance function is independent of the excitation level α.
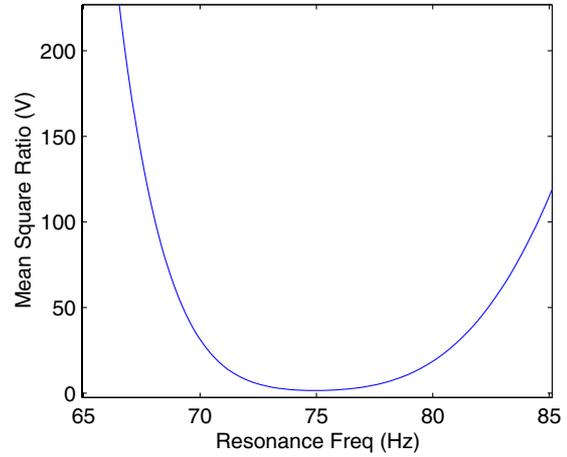
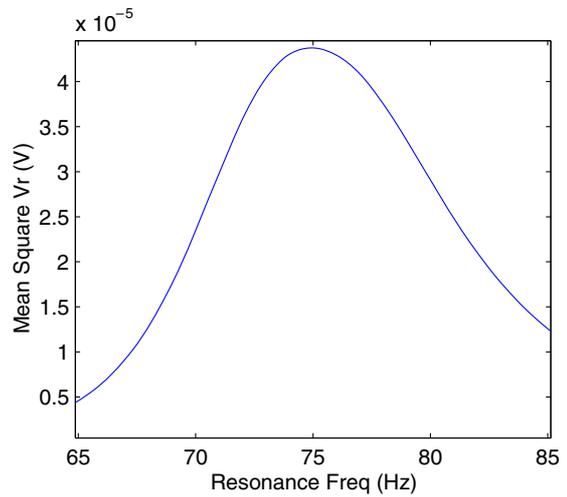**Figure 11.** The RMS ratio performance function.

Figure 12. The RMS value of V_R plotted against frequency.

4.4.2. Typical performance curves. Because of the analytic complexity of the performance functions, little is known of their properties. By simulation, both are insensitive to reasonable changes in damping ratio, but as expected, are strong functions of the branch resonance frequencies.

RMS strain. The surface is definitely not convex but appears to have a single global minima. The performance function is plotted against the resonance frequency of the second mode in figure 10. Over a certain modal frequency range the contribution from adjacent modes is small, allowing the performance function to be uncoupled into its modal components.

RMS ratio. The RMS ratio performance function is plotted in figure 11. As with the previous case, the function is non-convex but appears to have a single global minima. It should be noted that the minima of this function does not occur exactly at the minimum of RMS strain (in our case the approximation is correct to 0.01 Hz).

Hollkamp [5], suggests a performance function similar to (35) with the following exceptions: V_p is measured directly
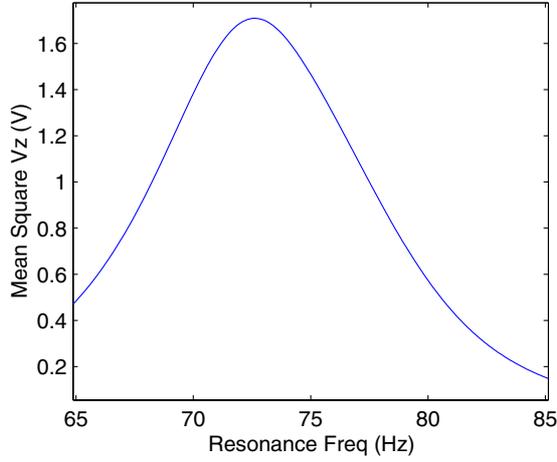
Figure 13. The RMS value of V_z plotted against frequency.

Figure 14. The variance of $V_k(\theta)$ plotted against the averaging length N.

from an additional piezoelectric patch, and the denominator is the RMS value of V_z. Figures 12 and 13 compare the RMS values of V_R and V_z. It can be seen that maximizing the RMS value of V_R is much more desirable than performing the same operation on V_z. These simulations were performed using damping ratios of $\varsigma = 0.005$ for each mode. As the damping ratios are increased, the approximation made by Hollkamp becomes more accurate, i.e. $\arg\max_{\theta \in \Re^{N_\omega}} E\{V_z^2(t)\}$ approaches $\arg\max_{\theta \in \Re^{N_\omega}} E\{V_r^2(t)\}$ as the structural damping ratios are increased.

4.4.3. Convergence. For some desired variance in $V_k(\theta)$ it is desirable to estimate the required length of the averaging interval. A large conservative N will result in a small variance but slow update rate. The opposite is true for an insufficiently small N, fast update but large variance.

We will consider only $V_k^{strain}(\theta)$: the analysis is easily extended to $V_k^{ratio}(\theta)$ by applying the technique to both the numerator and denominator. From [29]

$$\text{Var } V_k(\theta) = E\{V_k^2(\theta)\} - \overline{V_k(\theta)}^2 \qquad (37)$$

$$\text{Var } V_k(\theta) \approx \frac{4}{(NT_s)^2} \int_0^{NT_s} (NT_s - \tau) R_{v_p}^2(\tau) \, d\tau \qquad (38)$$

where

$$R_{v_p}(\tau) \approx \mathcal{F}^{-1}\{|G_{vv}(j\omega)|^2 S_U(\omega)\}. \qquad (39)$$

To be precise, the autocorrelation $R_{v_p}(\tau)$ is actually dependant on the closed loop transfer function $\tilde{G}_{vv}(j\omega)$, not $G_{vv}(j\omega)$ as shown in (39). For our purposes this (conservative) approximation is acceptable. Intuitively, equation (38) reveals that, as the structure becomes more resonant, we have to gather more data to maintain a constant variance on our performance function. As $G_{vv}(j\omega)$ becomes more resonant, the autocorrelation $R_{v_p}(\tau)$ is spread over τ. Equation (38) contains a convolution in $R_{v_p}^2(\tau)$, so the magnitude of the variance is increased.

Example: white noise disturbance. Consider a white disturbance applied to the actuator:
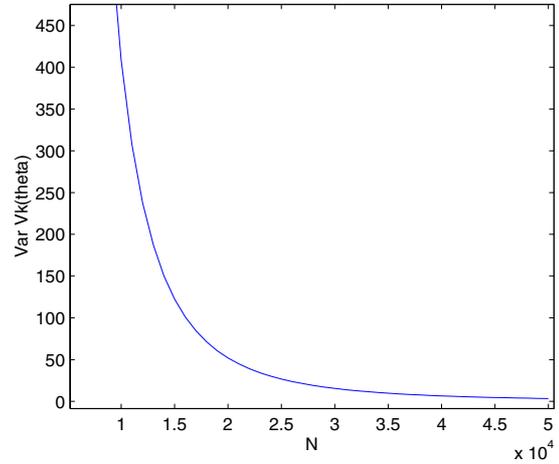
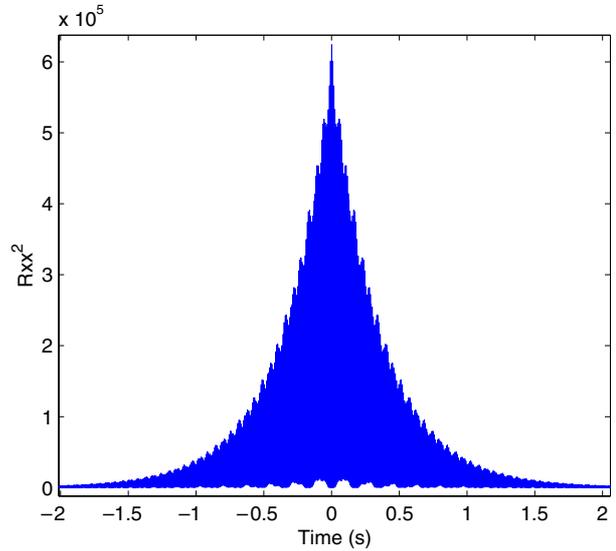$$S_{V_a}(\omega) = 1 \qquad (40)$$

Figure 15. Autocorrelation function.

$$S_{V_p}(\omega) = |G_{vv}(j\omega)|^2 \qquad (41)$$

$$R_{v_p}^2(\tau) = (\mathcal{F}^{-1}\{S_{V_p}(\omega)\})^2. \qquad (42)$$

$R_{v_p}(\tau)$ is easily evaluated numerically using the inverse discrete Fourier transform. The squared autocorrelation function is plotted in figure 15. Equation (38) can now be evaluated numerically for various values of N. Considering that $R_{v_p}(0) = 314.14$, a reasonable value for the variance of $V_k(\theta)$ is 10. The coordinate ($N = 34\,700$, Var $V_k(\theta) = 9.99$) is selected from figure 14, which corresponds to an interval of approximately 35 s.

4.4.4. Practical implementation. Large averaging lengths can cause problems in real time implementation as (32) requires a large buffer size and involves a heavy computational load at the end of each interval. Given a platform with high numerical accuracy (i.e. IEEE floating point arithmetic) a recursive alternative to (32) can be derived.
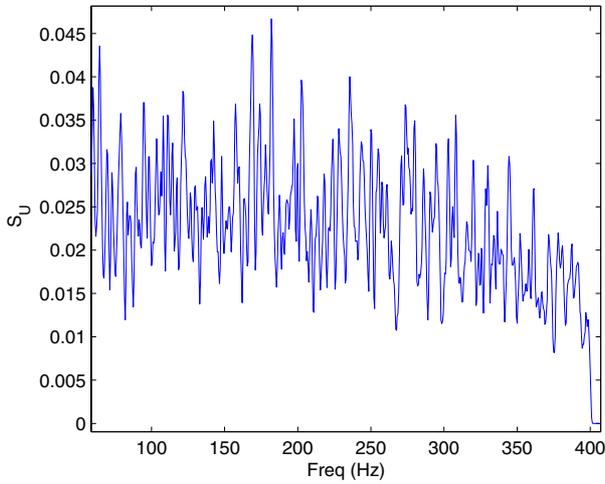
Figure 16. Excitation power spectrum.

Table 1. Experimental beam parameters.

Length, L (m)	0.6
Width, w_b (m)	0.05
Thickness, h_b (m)	0.003
Young's modulus, E_b (10^9 N m^{-2})	65
Density, ρ (kg m^{-2})	2650

We begin with the N term approximation:

$$E\{V_p^2\}_N = \frac{1}{N}\sum_{i=1}^{N} V_p^2(iT_s) \qquad (43)$$

which can be continued to the $N+1$ term approximation:

$$E\{V_p^2\}_{N+1} = \frac{1}{N+1}\sum_{i=1}^{N+1} V_p^2(iT_s) \qquad (44)$$

$$E\{V_p^2\}_{N+1} = \frac{1}{N+1}\sum_{i=1}^{N} V_p^2(iT_s) + \frac{1}{N+1}V_p^2((N+1)T_s). \qquad (45)$$

Noting that

$$NE\{V_p^2\}_N = \sum_{i=1}^{N} V_p^2(iT_s) \qquad (46)$$

equation (45) becomes

$$E\{V_p^2\}_{N+1} = \frac{N}{N+1}E\{V_p^2\}_N + \frac{1}{N+1}V_p^2((N+1)T_s). \qquad (47)$$

By again considering the N term approximation we arrive at the solution

$$E\{V_p^2\}_N = \frac{N-1}{N}E\{V_p^2\}_{N-1} + \frac{1}{N}V_p^2(NT_s). \qquad (48)$$

4.5. Searching the performance surface

Given that an estimate of the performance function is available, the parameter vector θ can be updated using a gradient search

Table 2. PZT properties.

Length (m)	0.070
Charge constant, d_{31} (m V^{-1})	-210×10^{-12}
Voltage constant, g_{31} (V m N^{-1})	-11.5×10^{-3}
Coupling coefficient, k_{31}	0.340
Capacitance, C_p (μF)	0.105
Width, $w_s w_a$ (m)	0.025
Thickness, $h_s h_a$ (10^{-3} m)	0.25
Young's modulus, $E_s E_a$ (10^9 N m^{-2})	63
Distance from beam end (m)	0.05

algorithm. Newton's method [27] is selected for its fast convergence:

$$\theta_{k+1} = \frac{V(\theta_k)(\theta_k - \theta_{k-1})}{V(\theta_k) - V(\theta_{k-1})}. \qquad (49)$$

For practical reasons the step size is artificially limited. Although this slows convergence, it provides needed robustness to gradient errors and numerical sensitivity at the minima. The real time implementation of the limited Newton search algorithm also contains a small artificial bias to maintain the algorithm if $\theta_k - \theta_{k-1} \approx 0$.

5. Experimental results

5.1. Experimental set-up

The experimental beam is a uniform aluminum bar with rectangular cross section and experimentally pinned boundary conditions at both ends. A pair of piezoelectric ceramic patches (PIC151) are attached symmetrically to either side of the beam surface. One patch is used as an actuator and the other as a shunting layer. Physical parameters of the experimental beam and PZTs are summarized in tables 1 and 2. Note that the location of the piezoelectric patch offers little control authority over the first mode. In this work, the structure's second and third modes are targeted for reduction.

The displacement and voltage frequency responses are measured using a Polytec laser vibrometer (PSV-300) and a HP spectrum analyzer (35670A).

The current source and buffer/amplifiers required for the synthetic impedance are constructed from Burr Brown OPA445 opamps. These opamps have a supply voltage limit of ±45 V. If necessary, the circuit can be constructed from high voltage opamps with supplies of greater than ±400 V.

5.2. Damping performance

To verify the function of the adaptive impedance a poorly tuned shunt circuit is applied to the experimental beam. This is equivalent to a large step change in the resonance frequencies of the structure. It is expected that the update algorithm will iteratively retune the parameters to minimize (32). In order to perform simulations, a frequency domain subspace algorithm [30, 31] is employed to obtain a tenth-order model for the two open-loop system transfer functions $G_{yv}(s)|_{x=0.17\text{ m}}$ and $G_{vv}(s)$. The excitation is a pseudo-random signal with fourth-order low pass cutoff at 400 Hz. The experimental 1000 average power spectrum is plotted in figure 16.
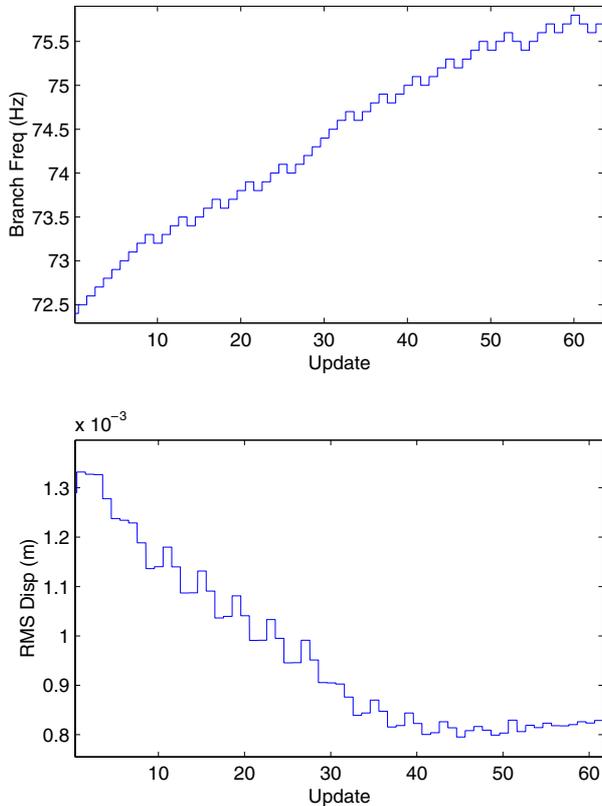
Figure 17. Experimental evolution of the second-mode branch frequency and modal displacement component ($x = 0.17$).

Figure 18. Experimental evolution of the third-mode branch frequency and modal displacement component ($x = 0.17$).

5.2.1. Performance function: RMS strain. A parameterized current blocking shunt circuit is applied to the beam. The evolution of the frequency tuned parameters and the RMS displacement for each mode is shown in figures 17 and 18. The corresponding time evolution of the second-mode frequency response is shown in figure 19.

A method is presented in [9] for finding shunt circuit component values that minimize the $\mathcal{H}_2$ norm of the displacement transfer function. This method can be used to find optimal component values that minimize (32). Figure 20 shows the theoretically predicted and experimentally adapted displacement frequency responses.

5.2.2. Performance function: RMS ratio. A parameterized current flowing shunt circuit [1, 14] is applied to the beam. The evolution of the frequency tuned parameters and the performance component of each mode is shown below in figures 21 and 22.

Because of the low gradients around the minima of this performance function, the resonance frequencies tend to drift slightly after adjustment. The low gradients cause the differences in consecutive updates of the performance function to be small over an attributable range of frequencies around the minima, see figures 21 and 22. Figure 23 shows the initial, adapted, and misadjusted displacement frequency responses of the beam. The frequency response (c) corresponds to the instance of peak misadjustment in the second-mode branch frequency.
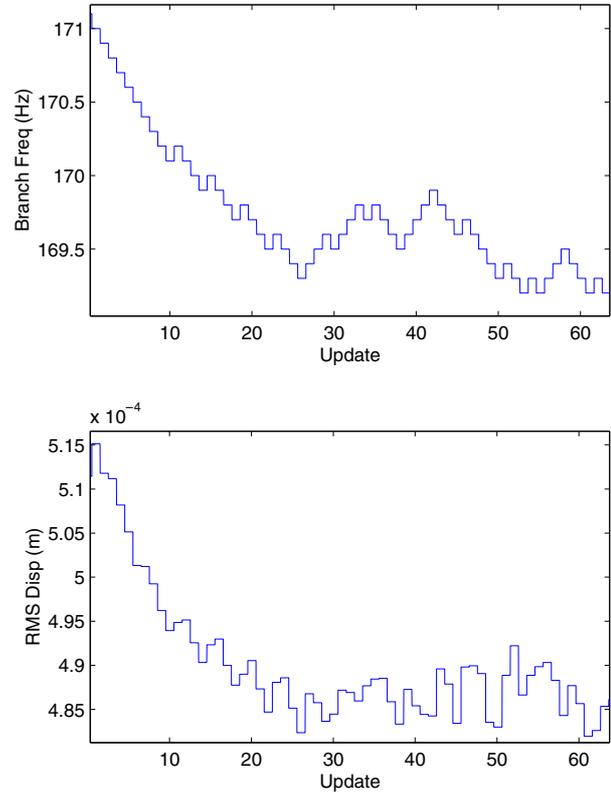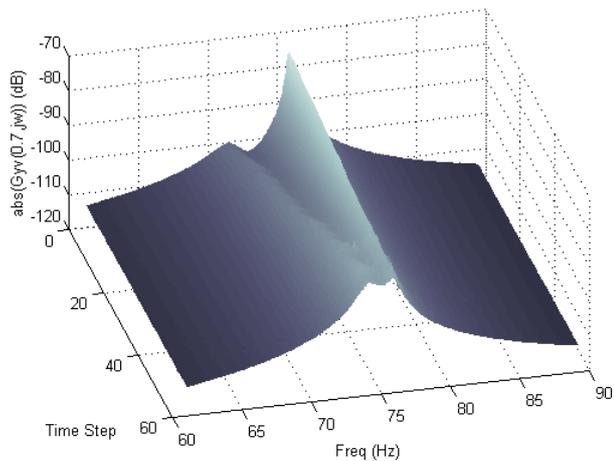

Figure 19. Experimental time evolution of the second-mode frequency response.

6. Conclusions

The performance of finely tuned piezoelectric shunt damping systems is extremely sensitive to the resonance frequencies of the host structure. The adaptive impedance allows us to retain the desirable characteristics of shunt damping systems, e.g. robustness, while automating the process of component tuning. The technique presented requires only a single patch. An understanding of the underlying feedback structure has allowed us to synthesize additional signals required for adaptation. Previously these signals have been obtained from additional patches or accelerometers.
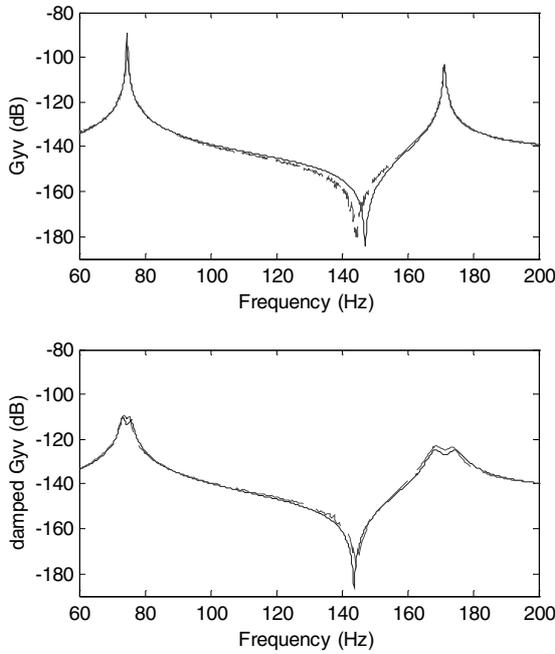
Figure 20. Open loop G_{yv} frequency response: (——) measured, ($\cdots$) subspace model. Adapted damped frequency response: (——) measured, ($\cdots$) simulated.
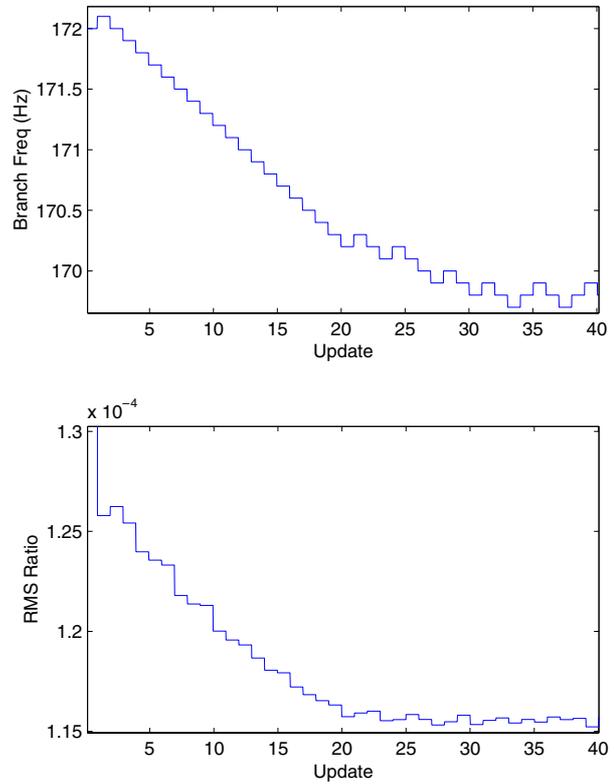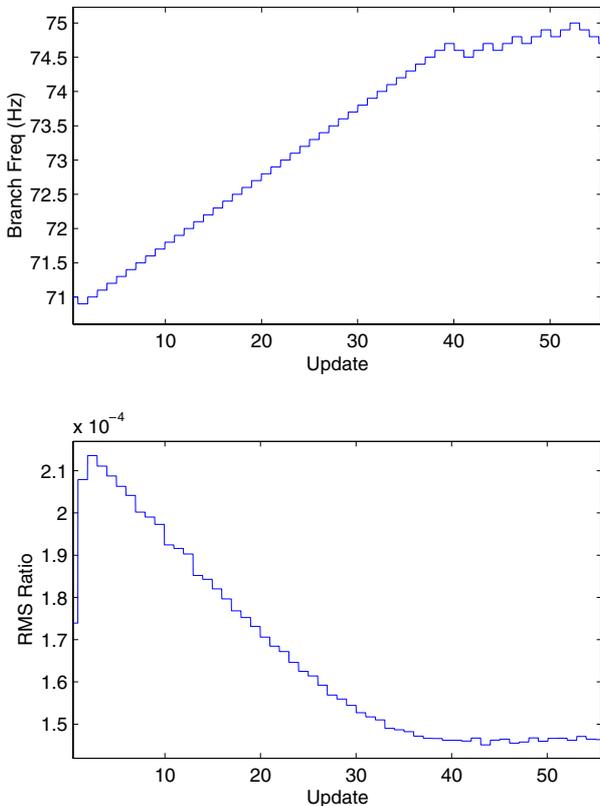

Figure 21. Experimental evolution of the second-mode branch frequency and RMS ratio performance function.

Two performance functions have been proposed:

- The RMS strain. By synthesizing the piezoelectric sensor voltage, it is possible to estimate the RMS strain under the PZT. This performance function provides reliable tuning

Figure 22. Experimental evolution of the third-mode branch frequency and RMS ratio performance function.

only if the disturbance is wide sense stationary. By simulation, the performance function appears to have a single global minima and can be minimized using the Newton search algorithm.

- The RMS ratio. Minimizing this performance function has the effect of minimizing the synthesized piezoelectric sensor voltage and maximizing the synthesized voltage across the shunting resistances. By simulation, it has a single global minima very close to the minima of the RMS strain. This function is independent of slow variations in the disturbance magnitude.

Experimental results show reliable estimation of the performance functions, optimal tuning of the circuit parameters, and satisfactory misadjustment. The synthetic impedance provides a near-ideal means for implementing the shunt circuits: the second and third modes are reduced in magnitude by up to 22 and 19 dB. Although both shunt circuit configurations (current blocking and current flowing) provide similar performance, the current flowing technique requires a lower-order admittance transfer function, and is easily parameterized in terms of the branch resonance frequencies. These reasons make the current flowing technique an ideal candidate for damping a large number of modes, as performed in [1].

Future work on the proposed adaptive scheme may involve a full analysis of the convergence properties. An attempt could also be made to estimate the disturbance, which appears to be difficult as the secondary path is a strong function of the parameter vector θ. It may also be possible, using small samples of open-loop operation, to estimate the resonance
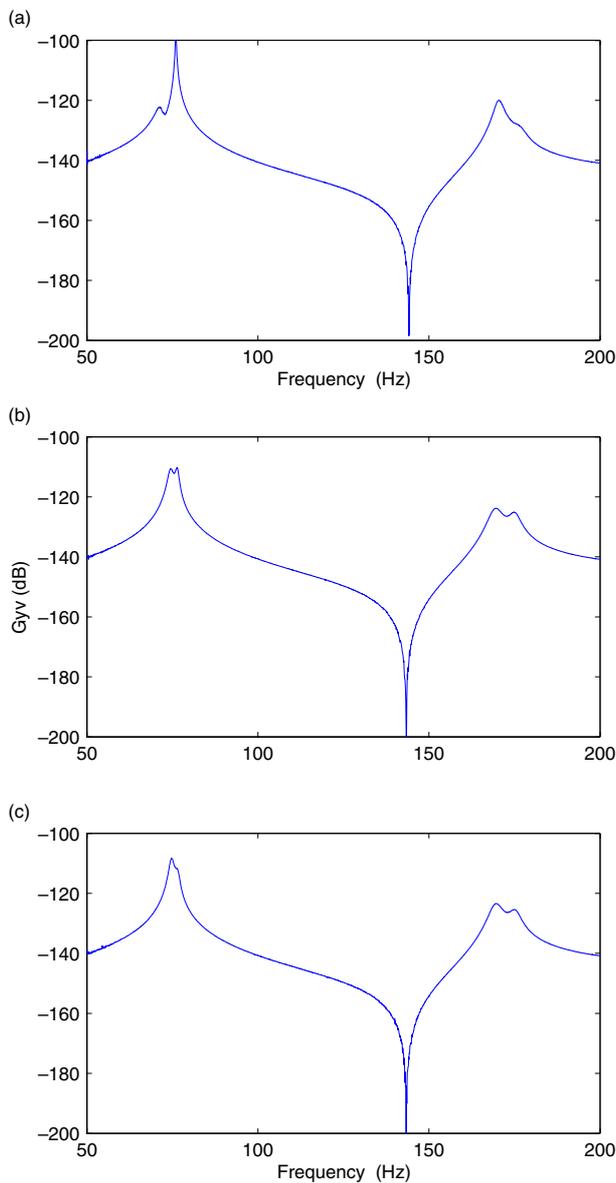
Figure 23. The measured transfer functions from applied voltage to structural displacement ($x = 0.17$ m). (a) Untuned, (b) at the minima, (c) peak misadjustment.

frequencies and damping ratios of each mode. If so, the optimal circuit parameters may be estimated in a single update period.

References

[1] Behrens S and Moheimani S O R 2002 Current flowing multiple mode piezoelectric shunt dampener *Proc. SPIE Smart Materials and Structures (San Diego, CA, March 2002); Paper No* 4697-24

[2] Hagood N W and Von Flotow A 1991 Damping of structural vibrations with piezoelectric materials and passive electrical networks *J. Sound Vib.* **146** 243–68

[3] Wu S Y 1998 Method for multiple mode shunt damping of structural vibration using a single PZT transducer *Proc. SPIE Smart Structures and Materials, Smart Structures and Intelligent Systems (Huntington Beach, CA, March 1998); SPIE* **3327** 159–68

[4] Smith K E, Maly J R and Johnson C D 1991 Smart tuned mass dampers *Proc. ADPA/AIAA/ASME/SPIE Conf. on Active Materials and Adaptive Structures (Alexandria, VA)* pp 19–22

[5] Hollkamp J J and Starchville T F Jr 1994 A self-tuning piezoelectric vibration absorber *J. Intell. Mater. Syst. Struct.* **5** 559–65

[6] Davis C L and Lesieutre G A 2000 An actively tuned solid-state vibration absorber using capacitive shunting of piezoelectric stiffness *J. Sound Vib.* **232** 601–17

[7] Fleming A J, Behrens S and Moheimani S O R 2000 Synthetic impedance for implementation of piezoelectric shunt-damping circuits *Electron. Lett.* **36** 1525–6

[8] Fleming A J, Behrens S and Moheimani S 2000 Innovations in piezoelectric shunt damping *Proc. SPIE Symp. on Smart Materials and MEM's, Smart Structures Amd Devices (Melbourne, Australia, Dec. 2000); SPIE* **4326**

[9] Fleming A J, Behrens S and Moheimani S O R 2002 Optimization and implementation of multi-mode piezoelectric shunt damping systems *IEEE/ASME Trans. Mechatron.* **7** 87–94

[10] Hagood N W and Crawley E F 1991 Experimental investigation of passive enhancement of damping for space structures *J. Guid. Control Dyn.* **14** 1100–9

[11] Wu S Y 1996 Piezoelectric shunts with parallel R–L circuit for structural damping and vibration control *Proc. SPIE Smart Structures and Materials, Passive Damping and Isolation (March 1996); SPIE* **2720** 259–69

[12] Wu S Y 1999 Multiple PZT transducers implemented with multiple-mode piezoelectric shunting for passive vibration damping *Proc. SPIE Smart Structures and Materials, Passive Damping and Isolation (Huntington Beach, CA, March 1999); SPIE* **672** 112–22

[13] Wu S Y and Bicos A S 1997 Structural vibration damping experiments using improved piezoelectric shunts *Proc. SPIE Smart Structures and Materials, Passive Damping and Isolation (March 1997); SPIE* **3045** 40–50

[14] Behrens S, Moheimani S O R and Fleming A J 2002 Multiple mode passive piezoelectric shunt dampener *Proc. IFAC Mechatronics (Berkeley, CA, Dec. 2002)*

[15] Hollkamp J J 1994 Multimodal passive vibration suppression with piezoelectric materials and resonant shunts *J. Intell. Mater. Syst. Struct.* **5** 49–56

[16] Riordan R H S 1967 Simulated inductors using differential amplifiers *Electron. Lett.* **3** 50–1

[17] Fuller C R, Elliott S J and Nelson P A 1996 *Active Control of Vibration* (New York: Academic)

[18] Ljung L 1999 *System Identification: Theory for the User* (Englewood Cliffs, NJ: Prentice-Hall)

[19] Meirovitch L 1996 *Elements of Vibration Analysis* 2nd edn (Sydney: McGraw-Hill)

[20] Janocha H 1999 Actuators in adaptronics *Adaptronics and Smart Structures* ed B Clephas (Berlin: Springer) ch 6

[21] Dosch J J, Inman D J and Garcia E 1992 A self-sensing piezoelectric actuator for collocated control *J. Intell. Mater. Syst. Struct.* **3** 166–85

[22] Edberg D L, Bicos A S, Fuller C M, Tracy J J and Fechter J S 1992 Theoretical and experimental studies of a truss incorporating active members *J. Intell. Mater. Syst. Struct.* **3** 333–47

[23] Won C C 1995 Piezoelectric transformer *J. Guid. Control Dyn.* **18** 96–101

[24] Hagood N W, Chung W H and Flowtow A v 1990 Modelling of piezoelectric actuator dynamics for active structural control *J. Intell. Mater. Syst. Struct.* **1** 327–54

[25] Kuo S M and Morgan D R 1996 *Active Noise Control Systems* (New York: Wiley)

[26] Moheimani S O R, Fleming A J and Behrens S 2002 On the feedback structure of wideband piezoelectric shunt damping systems *Proc. IFAC World Congr. (Barcelona, Spain, July 2002)*

[27] Widrow B and Stearns S D 1985 *Adaptive Signal Processing (Signal Processing Series)* (Englewood Cliffs, NJ: Prentice-Hall)

[28] Brown R G and Hwang P 1997 *Introduction to Random Signals and Applied Kalman Filtering* (New York: Wiley) ch 2.4

[29] Bendat J S and Piersol A G 1966 *Measurement and Analysis of Random Data* (New York: Wiley)

[30] Mckelvy T, Akcay H and Ljung L 1996 Subspace based multivariable system identification from frequency response data *IEEE Trans. Autom. Control* **41** 960–78

[31] McKelvey T, Fleming A J and Moheimani S O R 2002 Subspace based system identification for an acoustic enclosure *ASME J. Vib. Acoust.* **124** 414–19